Turbulent Wake of a Sinusoidal Cylinder with Large Spanwise Wavelength at Re = 3000

Y.F. Lin[1,3] and H.L. Bai[1,2]

[1]State Key Laboratory of Aerodynamics, Mianyang Sichuan 621000, China

[2]Shenzhen Graduate School, Harbin Institute of Technology, Shenzhen 518055, China

[3]Parsons Brinckerhoff (Asia) Ltd., Kowloon Bay, Kowloon, Hong Kong SAR

Abstract

Geometric modification of the shape of a slender cylinder has been previously proved to be one effective means to passively control turbulent wake and, consequently, to reduce drag force as well as suppress fluctuating lift force. For example, Lam and Lin [1] investigated the turbulent wake of a sinusoidal cylinder, taking into account effects of the wavelength (λ/D_m) and amplitude (a/D_m) of the sinusoidal wave. At $\lambda/D_m = 1.9$ and $a/D_m = 0.152$, they observed a large reduction in both the time-averaged drag (up to 18%) and the fluctuating lift (up to 94%). However, their simulation was run within a relatively small range of λ/D_m (≤ 3.333). The present work aims to investigate the effects of large λ/D_m (= 3.79–7.57) on the turbulent wake of a sinusoidal cylinder, with an attempt to uncover the underlying mechanisms responsible for the large force reduction/suppression by the geometric modification. Large eddy simulation (LES) was conducted at a Reynolds number of Re = 3,000. It was found that a large force reduction/suppression occurs at $\lambda/D_m = 6.06$. The turbulent wake of the sinusoidal cylinder with the optimal configuration was examined in detail, including vortex formation length, flow separation angle, and additionally generated vortices.

Introduction

Turbulent flow around a bluff-body has been prevalently seen in engineering applications such as tube bundles in heat exchangers, offshore struts, cable-stayed bridges, and high-rising buildings, etc. This flow involves fundamental issues in fluid dynamics research, e.g., shear layer interactions, vortex dynamics, fluid structures interference, vortex-induced vibration, and noise generation [2]. Slender cylinder may be considered as the basic model of a bluff-body and thus its relevant flow has attracted a great deal of attention so far. Geometric modification of the cylinder shape is one of the passive means to control the flow structure, which may consequently and beneficially lead to a reduction and/or suppression of fluid forces acting on the bluff body. A slender cylinder with its surface being modified to be sinusoidal along its span is called a sinusoidal wavy cylinder (referred to as sinusoidal cylinder hereinafter), and it has received a lot of works so far, e.g. [3-7].

Past experimental and numerical investigations have revealed that the near wake structures of a sinusoidal cylinder were significantly modified by the spanwise-varying geometry, which is alternately comprised of a geometric saddle and node. Ahmed and Bays-Muchmore [3] measured surface pressure distributions of a sinusoidal cylinder (with a circular cross-section) and conducted flow visualization of the near wake structures at a Reynolds number $Re = 5 \times 10^3 - 2 \times 10^4$, based on incoming free-stream velocity (U_∞) and the mean diameter (D_m) of the sinusoidal cylinder. The spanwise wavelength (λ) of the sinusoidal wave examined was $\lambda/D_m = 1.2 - 2.4$, with one fixed wave amplitude $a/D_m = 0.1$. Three-dimensional (3D) flow

separation lines and streamwise trailing vortex structures were observed near the geometric nodes, which is ascribed to the significant pressure gradients along the spanwise direction. Using laser-induced fluorescence (LIF) flow visualization technique, Lam et al. [5] observed in the streamwise-spanwise plane rib-like structures downstream of a sinusoidal cylinder (with a circular cross-section), with $\lambda/D_m = 2.273$ and $a/D_m = 0.091$ ($Re = 6 \times 10^2$). Further, time sequences of their LIF results showed that these evolving rib-like structures were in fact associated with stremwise vortices developed from the nodes. Recent numerical works by Lam and Lin [6] ($\lambda/D_m = 1.136 - 3.333$, $a/D_m = 0.091$ & 0.152, $Re = 3 \times 10^3$) and Lam and Lin [7] ($\lambda/D_m = 1.0 - 10.0$, $a/D_m = 0.02 - 0.30$, $Re = 60 - 150$) showed additional streamwise vorticities and vortices in the near wake of a sinusoidal cylinder.

A large reduction/suppression in fluid forces has been observed for a sinusoidal cylinder with the optimum geometries, owing to the great modification of the near wake structures. Bearman and Owen [4] measured the base pressure of a square-section cylinder with a sinusoidal frontal face ($\lambda/D_m = 3.5 - 5.6$ and $a/D_m \leq 0.25$, $Re = 4 \times 10^4$) and observed a large reduction in the mean drag (up to 30%) with $\lambda/D_m = 5.6$ and $a/D_m = 0.25$, compared to that of a smooth cylinder. Using a load cell, Lam et al. [5] measured the fluid forces acting on a sinusoidal cylinder with $\lambda/D_m = 1.45 - 2.27$ and $a/D_m = 0.091$ and 0.125 ($Re = 2 \times 10^4 - 5 \times 10^4$), the largest reduction in the mean drag (up to 20%) being achieved with an optimum $\lambda/D_m = 2.08$. They argued that the drag reduction may depend on the degree of obliqueness of the sinusoidal cylinder, i.e. $a/(\lambda D_{min})$, where D_{min} is the diameter of the saddle. In a large eddy simulation (LES), Lam and Lin [6] obtained a mean drag reduction of 18% with $\lambda/D_m = 1.9$ ($Re = 3 \times 10^3$). The significant reduction in the mean drag and suppression of the fluctuating lift obtained for a sinusoidal cylinder with the optimum $\lambda/D_m \approx 2.0$ were mainly ascribed to the stabilized near wake, the elongated vortex formation length, and the reduced TKE. Interestingly, Lam and Lin's [7] numerical investigation ($Re = 100 - 150$) has revealed that there were two troughs at $\lambda/D_m \approx 2.0$ and 6.0 in the variations of forces (including the mean drag and the fluctuating lift) with λ/D_m, with increasing λ/D_m from 1.0 to 10.0, that is, two optimum λ/D_m corresponding to a large force reduction/suppression were observed. However, whether the relatively large $\lambda/D_m \approx 6.0$ is the optimum one for the force reduction/suppression in the subcritical flow regime is still unknown.

This work aims to investigate the turbulent wake of a sinusoidal cylinder with a relatively large λ/D_m in the subcritical flow regime. In particular, to extend Lam and Lin's [6] work, 3D LES is employed for a sinusoidal cylinder with $\lambda/D_m = 3.79 - 7.57$ and $a/D_m = 0.152$ at $Re = 3 \times 10^3$.

Numerical Simulation Details

Figure 1 shows the model of a sinusoidal cylinder, along with the symbol designations. The coordinates x, y and z denote the streamwise, cross-stream and spanwise directions, respectively. The shape of the cylinder is described by the equation of a sinusoidal wave, i.e., $D_z = D_m + 2acos(2\pi z/\lambda)$, where D_z is the local diameter of the cylinder at z of its span, D_m [= $(D_{min} + D_{max})/2$] is the mean diameter of the cylinder, and a and λ denote the amplitude and wavelength of the sinusoidal wave, respectively. The axial location with the maximum and minimum local diameter D_{max} and D_{min} are called a 'node' and 'saddle', respectively. In this paper, the normalization of length scales (such as x, y, z, a and λ) is based on D_m, without otherwise stated.
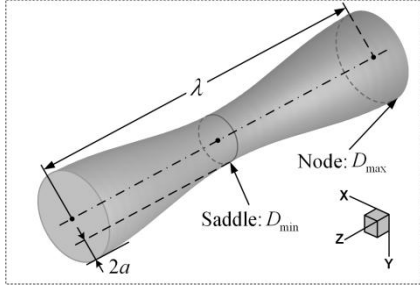

Figure 1. Schematic of the computational model. The mean diameter of the cylinder $D_m = (D_{max} + D_{min})/2$.

A total of six sinusoidal cylinder models (WY-I, WY-II, WY-III, WY-IV, WY-V and WY-VI) with different wavelength λ/D_m = 3.79, 4.55, 5.30, 6.06, 6.82 and 7.57 are presently investigated, given one fixed amplitude of the wave a/D_m = 0.152. A smooth circular cylinder with diameter D_m is considered, providing a baseline flow. All the simulations are carried out at a Reynolds number $Re = U_\infty D_m/\nu = 3 \times 10^3$, where U_∞ is the incoming free stream velocity and ν is the kinematic viscosity of fluid.

Similar to Lam and Lin [6], 3D LES is employed in the present work to solve the incompressible Navier-Stokes (N-S) equations on unstructured hexahedral grids. The filtered continuity and N-S equations in Einstein convention are as follows, respectively,

$$\frac{\partial \overline{u}_i}{\partial x_i} = 0, \tag{1}$$

$$\frac{\partial \overline{u}_i}{\partial t} + \frac{\partial \overline{u}_i \overline{u}_j}{\partial x_j} = -\frac{1}{\rho}\frac{\partial \overline{p}}{\partial x_i} + \nu \frac{\partial^2 \overline{u}_i}{\partial x_j \partial x_j} - \frac{\partial \tau_{ij}}{\partial x_j}, \tag{2}$$

$$i \in \{1,2,3\},$$

where $\overline{u}_i$ are the filtered velocity components along the corresponding Cartesian coordinates x_i, $\overline{p}$ is the flow pressure and ρ is the fluid density. The subgrid scale stress, τ_{ij}, is defined as $\tau_{ij} = \overline{u_i u_j} - \overline{u}_i \overline{u}_j$. The well known Smagorinsky model is adopted to model the subgrid scale, with the mixing length being defined as $l_s = \min (kh, C_s \Delta^{1/3})$, where k and C_s are the von Kármán and Smagorinsky constants, respectively, h is the distance from the wall and Δ is the volume of the cell. Presently, $C_s = 0.1$ [6]. The finite volume discretization of a second-order central scheme is applied for momentum discretization, while a second-order implicit scheme for temporal discretization. The velocity-pressure coupling is based on the PISO. More detailed descriptions and validation tests of the present 3D LES can be found in [6].

The computational domain ($L_x \times L_y \times L_z$) is chosen to be $L_x = 24D_m$, $L_y = 16D_m$ and $L_z = \lambda$, along the streamwise, cross-stream and spanwise directions, respectively. The same size of grid distribution was used by Lam and Lin [6]. The inlet boundary is at $8D_m$ upstream of the cylinder centre, with a constant and uniform velocity (i.e. U_∞) imposed. The outflow boundary is at $16D_m$ downstream of the cylinder centre and the convective boundary condition is used, i.e., $\partial u_i/\partial t + U_c(\partial u_i/\partial x) = 0$, where U_c (= U_∞) is the convective velocity. The 'no-slip' condition is applied to the cylinder surface.

Results and Discussions

Force Coefficients

Figure 2 presents variations with λ/D_m of the mean drag coefficient $\overline{C}_D$ and the fluctuating lift coefficient C'_L for the sinusoidal cylinders. Previous results of a smooth circular cylinder and sinusoidal cylinders with relatively small λ/D_m (= 1.14–3.33) obtained by Lam and Lin [6] using LES at $Re = 3 \times 10^3$ are included for comparison. The coefficients $\overline{C}_D$ and C'_L are defined as $\overline{C}_D = 2\overline{F}_D/(\rho U_\infty^2 D_m L_z)$ and $C'_L = 2F'_L/(\rho U_\infty^2 D_m L_z)$, respectively, where $\overline{F}_D$ is the time-averaged (mean) drag force and F'_L is the fluctuating lift force (rms value).
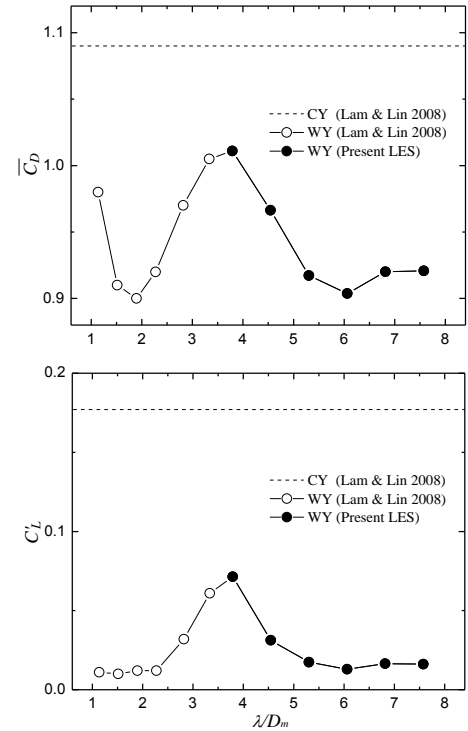

Figure 2. Dependence on λ/D_m of the time-averaged drag coefficient (upper) and fluctuating lift coefficient (lower). a/D_m = 0.152. Re = 3,000.

Evidently, $\overline{C}_D$ dips quickly with increasing λ/D_m from 1.14 to 1.89 and then climbs rapidly with further increasing λ/D_m from 1.89 to 3.33. The optimum wavelength corresponding to the maximum reduction of $\overline{C}_D$ occurs at λ/D_m = 1.89 in the relatively small λ/D_m-range (< 3.5) [6]). Meanwhile, at the relatively large λ/D_m-range examined in the present work, $\overline{C}_D$ declines again rapidly with increasing λ/D_m from 3.79 to 6.06 and then grows slowly with further increasing λ/D_m from 6.06 to 7.57. Thus, the second optimum wavelength of λ/D_m = 6.06 has been observed for the sinusoidal cylinder with the relatively large λ/D_m (= 3.79–7.57), with the maximum reduction of $\overline{C}_D$ by up to 16% being achieved in a comparison to that of the smooth circular cylinder. Load-cell measurements performed by Lam et al. [8] for a sinusoidal cylinder with $\lambda/D_m = 6$ and $a/D_m = 0.15$ at $Re = 6.8 \times 10^3–1.34 \times 10^4$ indicate a drag reduction up to 18%, compared with that of a smooth circular cylinder, providing a good validation for the present LES data. As a result of that, the variation of $\overline{C}_D$ with λ/D_m exhibits two valleys in Fig. 2, i.e., one

is located at $\lambda/D_m = 1.89$ and another at $\lambda/D_m = 6.06$ where significant reduction in the mean drag was achieved. Similar results were observed by Lam and Lin [7] in their numerical simulation, though in the laminar flow regime ($Re = 100$).

Further, C'_L is markedly reduced for the sinusoidal cylinders with the wavelength $\lambda/D_m = 1.14$–7.57, compared with that of a smooth circular cylinder. In particular, significant reduction up to 94% has been observed in both the lower range of $1.14 \le \lambda/D_m \le 2.27$ and the larger range of $5.3 \le \lambda/D_m \le 7.57$. This suggests pronounced suppression of the fluctuating lift at these λ/D_m-ranges. In the laminar flow regime ($Re = 100$), Lam and Lin [7] observed the significantly reduced C'_L in the larger λ/D_m-range, but not in the lower λ/D_m-range. Based on the behaviors of $\overline{C}_D$ and C'_L in Fig. 2 (open symbols), Lam and Lin [6] speculated that the vortex structures in the near wake was mainly modulated by the steepness of the sinusoidal wave, i.e. a/λ; the larger a/λ, corresponding to the smaller λ given a fixed a, may result in the more stabilized near-wake vortex structures and thus greater suppression of the fluctuating lift. However, the present observations for the sinusoidal cylinders with the relatively large λ/D_m (closed symbols in Fig. 2) may imply that the wave steepness a/λ is not directly associated with either the mean drag reduction or the fluctuating lift suppression.

Vortex Formation Length

The vortex formation length in the near wake of a slender cylinder is connected to the base pressure and thus the drag force. Therefore, it is important to quantify the vortex formation length of the sinusoidal cylinders in the present work. Here we define the time-averaged vortex formation length L_f as the distance between the cylinder centre and the location where time-averaged streamwise velocity $\overline{u}/U_\infty = 0$ along the wake centreline. Fig. 3 presents the L_f of three typical sinusoidal cylinders (WY-II, WY-IV and WY-VI), together with that of a smooth circular cylinder. Obviously, the vortex formation lengths of the sinusoidal cylinders are largely longer than that of the smooth circular cylinder; the sinusoidal cylinder WY-IV with $\lambda/D_m = 6.06$, which is the optimum wavelength for drag reduction (Fig. 2), has the longest L_f along the entire span from the node location ($z/\lambda = 0$) to the saddle location (0.5). Further, the vortex formation lengths of the sinusoidal cylinders, particularly the two with larger λ/D_m, exhibit large variations from the nodal location to the saddle location along the spanwise direction; the L_f retreats from the nodal location to the saddle location along the spanwise direction, leading to a longer L_f at the nodal location than at the saddle location. These observations are completely opposite to that by Lam and Lin [6] for the sinusoidal cylinders with the relatively small λ/D_m (= 1.14–2.27), given the same wave amplitude $a/D_m = 0.152$ and Reynolds number $Re = 3 \times 10^3$. That is, for the sinusoidal cylinders with the relatively small λ/D_m (= 1.14–2.27), the vortex formation length increases from the nodal location to the saddle location along the spanwise direction, thus it is longer at the saddle location than at the nodal location. This reversed change of the vortex formation length from the nodal location to the saddle location was also observed by Lam and Lin [7] in the laminar flow regime ($Re = 100$), who ascribed this change to the flow separation characteristics and the near-wake structure organizations for different wavelengths.

It is well known that the mean drag coefficient $\overline{C}_D$ is proportional to the negative base pressure coefficient in the subcritical flow regime. And the vortex formation length of a circular cylinder was inversely proportional to the mean base pressure coefficient [2]. Therefore, an elongated vortex formation length is corresponding to a reduced mean drag coefficient. This is also true for the case of the sinusoidal cylinder as has been confirmed. As discussed above, two optimum wavelengths λ/D_m

≈ 2.0 and 6.0, in terms of force reduction/suppression, have been observed for the sinusoidal cylinders, with λ/D_m being varied from 1.0 to 10.0, based on the previous and our investigations; the longest vortex formation length is formed by the sinusoidal cylinder with the optimum λ/D_m. On another comment, all the vortex formation lengths of the sinusoidal cylinders with $\lambda/D_m = 1.14$–7.57, given $a/\lambda = 0.152$, are larger than that of the smooth circular cylinder ($Re = 3 \times 10^3$), which may explain the drop of the mean drag coefficient $\overline{C}_D$ in the entire wavelength range concerned presently in Fig. 2.
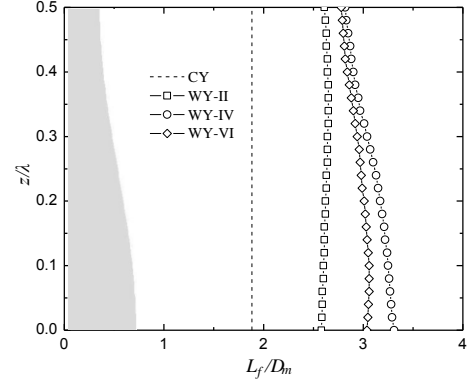

Figure 3. Vortex formation lengths (L_f/D_m) of the sinusoidal cylinders (WY-II: $\lambda/D_m = 4.55$; WY-IV: 6.06; WY-VI: 7.57) from node ($z/\lambda = 0$) to saddle (0.5) at $y/D_m = 0$. Grey zone indicates a part of the sinusoidal cylinder.

Flow Separation Angles

Flow separation angle is an indicator of flow separation point or line where surface shear stress vanishes. Fig. 4 shows spanwise variations of the flow separation angles of three typical sinusoidal cylinders (WY-II, WY-IV and WY-VI). The flow separation angle of a smooth circular cylinder, $\theta_{sep} = 88^o$, is denoted by the dashed line for comparison. In general, the flow separation angles of the sinusoidal cylinders along the entire span are larger than that of the smooth circular cylinder. That is, the flow separation around the sinusoidal cylinders is postponed, compared with that around the smooth circular cylinder. Meanwhile, the flow separation angles of the sinusoidal cylinders display large variations along the spanwise direction from the nodal location ($z/D_m = 0$) to the saddle location (0.5). For the sinusoidal cylinder WY-II with $\lambda/D_m = 4.55$, the flow separation angle is largest ($\theta_{sep} = 91.5^o$) at the nodal location and declines gradually when moving towards the saddle location. This observation is consistent with that by Lam and Lin [6] for the sinusoidal cylinder with the relatively small λ/D_m (< 3.5). The large spanwise variation of the flow separation angle may result in the wavy fashion of flow structures in the near wake [3]. On the contrary, for the sinusoidal cylinder with $\lambda/D_m = 6.06$, the flow separation angle varies little from the nodal location to the saddle location. With further increasing the wavelength, the flow separation angle of the sinusoidal cylinder with $\lambda/D_m = 7.57$ changes differently from that of the sinusoidal cylinder with $\lambda/D_m = 4.55$, that is, the flow separation angle of the former increases but that of the latter decreases progressively along the span from the nodal location to the saddle location. At the saddle location, the flow separation angle of the sinusoidal cylinder with $\lambda/D_m = 7.57$ is about 89°, larger than that of other two sinusoidal cylinders and the smooth circular cylinder. Based on the above observations, we can see that the sinusoidal cylinder with $\lambda/D_m = 6.06$, which is the optimum wavelength for drag reduction (Fig. 2), has the spanwise-invariable flow separation angle, akin to that of the smooth circular cylinder. This may suggest that the vortex structures in the near wake generated by the sinusoidal cylinder with the optimum λ/D_m (= 6.06) be more stable than that by other

two, thus resulting in the longer vortex formation length (Fig. 3) and the smaller mean drag and fluctuating lift (Fig. 2).
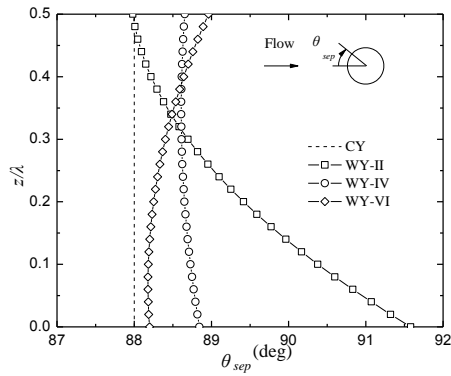

Figure 4. Flow separation angles (θ_{sep}) around the sinusoidal cylinders (WY-II: $\lambda/D_m = 4.55$; WY-IV: $\lambda/D_m = 6.06$; WY-VI: $\lambda/D_m = 7.57$) from node ($z/\lambda = 0$) to saddle ($z/\lambda = 0.5$).

Three-dimensional Vortex Structures

The 3D vortex structures in the near wake of the sinusoidal cylinder with the optimum $\lambda/D_m = 6.06$ are examined, in order to gain some insight into the underlying mechanism that leads to the large drag reduction and fluctuating lift suppression. Fig. 5 shows the iso-surfaces of normalized instantaneous spanwise, streamwise and transverse vorticity. It can be seen that the iso-surfaces of the spanwise vorticity display immediately downstream of the cylinder the wavy fashion along the spanwise direction, indicating a strong 3D development of the shear layers separating from the cylinder surface. The 3D shear layers appear stable and difficult to roll up to form the mature vortices. Therefore, the further downstream vortex shedding occurs in the near wake of the sinusoidal cylinder with $\lambda/D_m = 6.06$, resulting in a longer vortex formation length, compared to that of the smooth circular cylinder. Similar observations were made by Lam and Lin [6, 7] in both laminar and subcritical flow regimes.
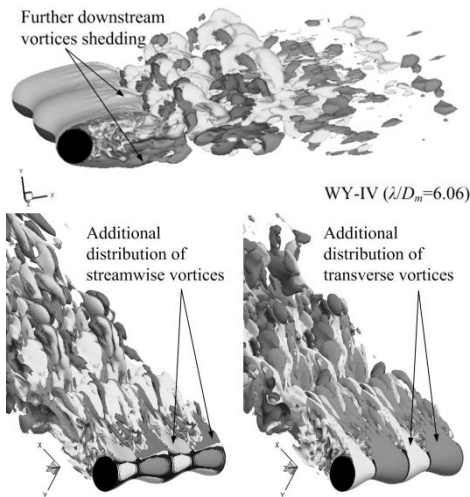

Figure 5. Iso-surfaces of instantaneous spaniwise (upper, $\omega_z = \pm 1$), streamwise (lower left, $\omega_x = \pm 1$) and transverse vorticity (lower right, $\omega_y = \pm 1$) of the sinusoidal cylinder with $\lambda/D_m = 6.06$.

Further, there exist additional streamwise and transverse vortices in the near wake of the sinusoidal cylinder. These vortices, generated by the periodic modification of the cylinder surface, exhibit the periodicity along the spanwise direction and play a role in modifying the flow structures in the near wake. Apparently, the spanwise alignment of these additional vortices and thus their role in the alteration of the near wake structures depend on the wavelength and amplitude of the sinusoidal wave. Here, based on the observations in the present and previous investigations, we surmise that the additionally generated streamwise vortices in the near wake by the sinusoidal cylinder with the optimum $\lambda/D_m \approx 6.0$ could stabilize to the greatest extent the shear layers, retarding their development to roll up into the mature vortices and thus resulting in the most elongated vortex formation length.

Conclusions

3D LES work was carried out at $Re = 3 \times 10^3$ to examine the turbulent wake of a sinusoidal wavy cylinder with $\lambda/D_m = 3.79$-7.57, given a fixed $a/D_m = 0.152$, with a view to extending previous studies and gaining some insight into the mechanism that leads to the large drag reduction and fluctuating lift suppression. It has been found that the great force reduction/suppression can be obtained at a large $\lambda/D_m \approx 6.0$. This is ascribed to the longest vortex formation length formed and the spanwise-invarying flow separation angle of the sinusoidal cylinder with the optimum wavelength. Comparison between the present work and previous investigations in the relatively small range of λ/D_m is provided.

References

[1] Lam, K. & Lin, Y.F., Large eddy simulation of flow around wavy cylinders at a subcritical Reynolds number, *International J. of Heat and Fluid Flow*, 29, 2008, 1071-1088.

[2] Williamson, C.H.K., Vortex dynamics in the cylinder wake, *Annual Review of Fluid Mech.*, 28, 1996, 477-539.

[3] Ahmed, A. & Bays-Muchmore, B., Transverse flow over a wavy cylinder, *Phys. of Fluids A*, 4(9), 1992, 1959-1967.

[4] Bearman, P.W. & Owen, J.C., Reduction of bluff-body drag and suppression of vortex shedding by the introduction of wavy separation lines, *J. of Fluids and Structures*, 12 1998, 123-130.

[5] Lam, K., Wang, F.H., Li, J.Y. & So, R.M.C., Experimental investigation of the mean and fluctuating forces of wavy (varicose) cylinders in a cross-flow, *J. of Fluids and Structures*, 19, 2004, 403-417.

[6] Lam, K. & Lin, Y.F., Large eddy simulation of flow around wavy cylinders at a subcritical Reynolds number, *International J. of Heat and Fluid Flow*, 29, 2008, 1071-1088.

[7] Lam, K. & Lin, Y.F., Effects of wavelength and amplitude of a wavy cylinder in cross-flow at low Reynolds numbers, *J. of Fluid Mech.*, 620, 2009, 195-220.

[8] Lam, K., Lin, Y.F., Zou, L. & Liu, Y., Experimental study and large eddy simulation of turbulent flow around tube bundles composed of wavy and circular cylinders. *International J. of Heat and Fluid Flow*, 31, 2010, 32-44